Experimental evaluation of the effect of cement type and seawater salinity on concrete offshore structures

Marinelle El-Khoury, Emmanuel Roziere, Frederic Grondin, Rachid Cortas, Fadi Hage Chehade

Experimental evaluation of the effect of cement type and seawater salinity on concrete offshore structures

Marinelle El-Khoury[1, 2], Emmanuel Roziere[1*], Frederic Grondin[1], Rachid Cortas[3], Fadi Hage Chehade[2]

[1] *Civil engineering and Mechanics Research Institute (GeM), UMR 6183, Centrale Nantes – Université de Nantes - CNRS, 1 rue de la Noë 44321 Nantes, France.*

[2] *Centre de Modélisation, Ecole Doctorale des Sciences et Technologie, Université Libanaise, Lebanon.*

[3] *Centre de Recherches Scientifiques en Ingénierie (CRSI), Université Libanaise, Beyrouth, Lebanon.*

[*] *Corresponding author.*

E-mail addresses: marinelle.el-khoury@ec-nantes.fr (M. El-Khoury); *emmanuel.roziere@ec-nantes.fr* (E. Roziere); *frederic.grondin@ec-nantes.fr* (F. Grondin); *rachid.cortas@gmail.com* (R. Cortas); *fchehade@ul.edu.lb* (F. Hage Chehade).

Summary

Although seawater exposure is relatively common, there are relatively few studies that couple the microscopic characterization to the mechanical/ macroscopic behavior of cement-based materials, by using a reformulation of seawater with all its multiple salts in the laboratory. The experimental study includes the effect of salinity, cement type, and specimens geometry on the degradation phenomenon. The seawater solution was recomposed in the laboratory by dissolving salts in deionized water. A stable brucite layer and calcium carbonate were formed at the surface of the exposed specimen. Continuous leaching of calcium hydroxide and formation of Friedel's salt was also observed. The mechanical properties of the attacked specimens remain equal or slightly lower than the control specimens even if significant changes could be observed in the microstructure. Due to seawater exposure, the hollow cylinders recorded the highest mass and volume gain thus the largest amount of products formed. These evolutions were accelerated with the increase of salinity contrariwise to expansion that was not affected by salinity increase and remained minor. Ordinary Portland cement recorded higher volume and weight gain than seawater resisting cement.

Key words

Durability, cement, offshore structures, seawater, salinity, microstructure, brucite, Friedel's salt.

1. Introduction

The offshore engineering sector is growing rapidly, supporting the use of concrete in marine environments. The durability of offshore concrete structures should be carefully assessed to avoid catastrophic failure especially in the oil and gas sector where these failures are followed by explosions, a huge gas leak in seawater, seawater contamination, loss of wildlife, and economical issues. Based on a worldwide study done on more than 380,000 wells from Canada, China, Netherlands, Offshore Norway, UK, and the US, seven percent of wells recorded integrity failures [1]. Another example can highlight the relevance of the study. The rebuilding of Beirut's port after the dramatic explosion in 2020 needs a quick process, but simultaneously, the quality and safety of the structures should be considered. Therefore, studying the concrete durability in marine environments is crucial for tackling social and environmental issues.

The corrosion of steel reinforcement is a major issue for reinforced concrete (RC) structures exposed to seawater. Three main zones can be distinguished, namely: atmospheric, splash/tidal, and submerged. Various previous studies have focused on the corrosion of steel due to the chloride ions diffusion [2,3] in harsh environments, and on the effect of wetting and drying (tidal zone) on concrete durability [4,5]. The purpose of this study was to focus on the cover of fully immerged RC structures and to check the chemical and microstructural stability of cement-based materials exposed to seawater. If the concrete cover is chemically attacked by seawater, this actually questions its ability to protect the steel reinforcement from corrosion. In seawater a diffusion-reaction phenomenon takes place in concrete between cement hydration products, pore solution, and seawater ions. The seawater environment and its effect on the chemistry and phase changes of cementitious materials are complex due to the presence of multiple salts. Sodium, chloride, magnesium, and sulfate are the major ions present in the seawater environment. Multiple works have focused on studying the effect of the external sulfate attack [6–8] and chloride diffusion [9–12] on concrete.

Several studies took into account the complexity of the combined chemical attack resulting from a combination of all the ions present in seawater environments [13,14] especially by performing in situ exposures in natural seawater sites [14,15]. The combined ions and their reaction with concrete phases can create a competition between protective layers formations and degradation and expansion due to ettringite formation [16]. Seawater attack is significantly different from sulfate attacks at equivalent sulfate concentration [13]. Therefore, while assessing the durability of concrete structures in seawater environment, all ions present in the seawater should be taken

into consideration. However, to limit the trouble of transporting structures to seawater sites, a laboratory investigation is used.

To study the phases change in the concrete, a specimen was immersed in the tidal zone at the Trondheim Fjord [14] and the results showed a layered attack caused by the combination of reactions that cannot be neglected. Seawater is paradoxically considered as less harmful for cement-based material than the chemical attacks due to each ion such as external sulfate attack, magnesium attack, chloride diffusion, etc.

Most of existing studies show significant expansion and strength loss associated to the influence of sulfate ions when using Portland cement [13,14]. Previous studies on seawater reported significant expansion and strength loss [13,17–20] of Portland cement based materials exposed to seawater attack, even if this is considered as less aggressive than external sulfate attack. However, these conclusions can be questioned when considering low-expansion or sulfate resistant cements with a composition complying with the provisions for seawater resistance provided by standards. There are very few studies related to the influence of clinker composition on the resistance to seawater attack, and the behavior of sulfate resistant Portland cement based materials exposed to seawater.

Few studies consider all the ions present in seawater. Most of the existing studies used natural seawater [14,21] and/or focused on the microstructural changes without coupling the phases changes with the mechanical behavior of the structure. Therefore, there are relatively few provisions on the composition of cement-based materials and durability testing procedures to anticipate their resistance to seawater exposure. Thus the interest and the novelty of the study also consist in providing alternative indicators and a comprehensive characterization to assess the strength of Portland-cement based materials to seawater.

Seawater chemical composition and salinity vary depending on the region, and it is difficult to measure the amount of salt dissolved in a seawater sample [22] and especially by drying and weighing [23]. Therefore, this study aims to expose cementitious materials to seawater solutions in the laboratory. Its composition and salinity are maintained constant all over the testing period. Definitions and units for the salinity across history have been previously studied and presented [24–26] and it is now known that the reference seawater normalized to a practical salinity of 35 has a Reference-Composition Salinity of exactly 35.16504 g/kg [22]. In this study, a useful method was used to study the seawater attack and the effect of salinity increase on concrete structures. This method limits the trouble of transporting samples to seawater sites and maintains the same chemical composition and salinity for the exposure solutions all over the testing

duration. It consists in recomposing the seawater solution in the laboratory, by dissolving multiple salts in deionized water [27] and the exposure solution was renewed every 14 days. Previous studies done using artificial salts in the laboratory focused mainly on studying the tidal zone [28], however fully immerged structures are analyzed in this paper. The age of exposure is an important aspect and it was also taken into consideration. Previous laboratory investigations focused on exposing structures to seawater at 28 days [28,29], however, in this study specimens have been exposed to artificial seawater at a relatively early age.

Therefore, the novelty of the study focuses on combining experimentally all the ions present in seawater in order to highlight their competition at the microscopic, macroscopic, and mechanical levels. Mortar specimens were immersed in tap water and in two exposure solutions with different salinities: 35g/L, representing the salinity of reference seawater, and 70 g/L, representing the double of the salinity of reference seawater. Two salinities were studied to check the effect of salinity increase in accelerating the attack process. To identify also the effect of cement type on seawater attack, two types of cement were examined in this study: Ordinary Portland Cement and another Portland Cement considered as resistant to seawater according to Sadran's index, defined as the sum of C_3A and $0.27C_3S$ contents. First, the detailed experimental program is given concerning the materials, the exposure conditions, and the testing procedures used to characterize the samples at different scales. Then, the results are analyzed and discussed. Three levels of characterization are detailed:

- Microstructural investigation using advanced techniques such as X-ray diffraction (XRD), thermogravimetric analyses (TGA/DTG), scanning electron microscopy (SEM) visualizations, and energy dispersive spectroscopy (EDS).
- Macroscopic analyses using volume, radius, and weight variations.
- Mechanical evaluations using compressive strength and Young's modulus evolutions.

Therefore, the effect of cement type, Sadran's index, seawater salinity and specimen shape are evaluated. This is achieved by immerging mortar specimens of different geometries, made with different cements, at a relatively early age (3 days) in multiple exposure solutions.

2. Experimental program

2.1. Materials and mixtures preparation

Mortar has been adopted as an alternative to concrete in multiple studies because it accelerates the testing process [6,30]. The maximum particle size thus the representative volume is lower. This allows reducing the characteristic time of diffusion, but the phenomena occurring at the

paste-aggregate interface can be taken into account. The investigation examines mortars made with an Ordinary Portland Cement (OPC) of type CEM I 52.5 N ("CEM I" in the results) and another cement CEM I 52.5 N PM ("PM" in the results) considered as resistant to seawater attack according to French standard NF P 15-317. Both types of cement are commercial products and the second one is actually used for structural concrete in marine environments. The water-to-cement (w/c) ratio of 0.6 was higher than the NF EN 206 recommendations [31] for seawater exposure. This value was adopted to accelerate the seawater attack by accelerating the diffusion of ions into the cement matrix. Siliceous sand (0-2mm) was used to avoid leaching and the reactions due to the presence of calcium carbonate in the case of limestone aggregates [32,33]. The sand had a fineness modulus of 2.6, a density of 2.61 and a coefficient of water absorption of 0.44%. Based on the particle size distribution and the shape of sand particles, preliminary tests have been performed to assess the paste volume in order to obtain a workable mortar. The composition of mortar mixture and the mineralogical composition of Portland Cement are summarized in Table 1.

Table 1: Mortar mix and cement mineralogical composition.

Mortar mixture composition		
Cement	500 kg/m^3	
Water	307 kg/m^3	
W/C	0.60	
Sand	1305 kg/m^3	
Cement composition		
	CEMI 52.5 N	**CEMI 52.5 N PM**
C_3S	60.0%	58.3%
C_2S	16.3%	17.5%
C_3A	7.7%	7.1%
C_4AF	10.5%	10.6%
Gypsum	3.5%	4.5%
Other contituents	2%	2%
Cement properties		
Density (10^3 kg/m^3)	3.16	3.18
Blaine fineness (m^2/kg)	400	430
Sadran's index ($C_3A+0.27C_3S \leq 23.5$)	**23.9 (not valid)**	**22.4 (valid)**

Two criteria were used to check if the studied types of cement were *a priori* resistant to seawater or not. The first criterion is based on Sadran's index [34]. This criterion has been retained in

French standard NF P 15-317 on “Hydraulic binders – Sea-water resisting cements”. If cement composition gives a Sadran’s index $C_3A+0.27C_3S$ lower than 23.5 it can be labeled as “sea setting” (PM) and therefore used in marine constructions. The second criterion is based on the C_3A content: For seawater-resistant cement, C_3A content should be lower than 8% [35].

The mortar mixtures were prepared in accordance with the NF EN 196-1 standard [36]. Tap water was used as mixing water to cast all the samples. The hollow and plain cylindrical specimens had a height of 160 mm and an external diameter of 70 mm. The internal diameter of hollow specimens was 30 mm, which implied a mortar thickness of 20 mm. The hollow cylindrical specimens allow accelerating the ions diffusion due to seawater attack. The specimens were stored for 24 hours in their molds at 20°C and 90% relative humidity. Then, they were demolded and a resin waterproof epoxy layer was applied on both circular end surfaces of the specimens. At the age of 48 hours, a second epoxy layer was applied. The aim of the resin layer on both ends of the cylinder was to obtain a two-dimensional diffusion of ions. At the age of 3 days, some specimens were immersed in exposure solutions and others in tap water. The geometries and dimensions of mortars specimens are illustrated in Fig. 1.

Gage studs and perforated plates were used in plain and hollow mortars, respectively, to measure the longitudinal deformation. Gage studs were inserted into the molds before casting. Plates were glued (without epoxy application) at the age of 24 hours after cutting and polishing the two circular end surfaces of concrete. The perforations maintain the solution circulation inside the sample. The total height of the specimen with the glue and the plates was 160 mm.

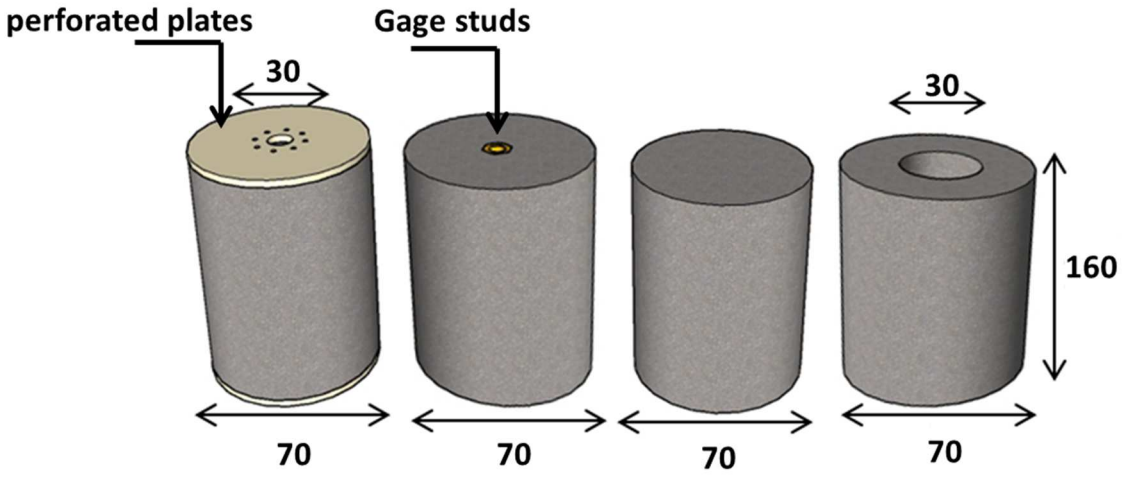

Fig. 1: Geometries and dimensions (mm) of mortars specimens: hollow cylinders (on both sides) and plain cylinders (center)

2.2. Exposure conditions

Seawater is a complex environment containing multiple ions; its chemical composition and salinity vary depending on the region. Data on multiple oceans' salinity, temperature, alkalinity, and pH can be found in [37] based on the global ocean data analysis project data set. Reference seawater normalized to a practical salinity of 35 has a Reference-Composition Salinity of exactly 35.16504 g/Kg [22].

A convenient method was used in this study to limit the trouble of transporting samples to seawater sites and to eliminate the problem of determining the seawater composition and salinity and its evolution with weather and time. The method consists of reformulating the seawater solution in the laboratory, by dissolving multiple salts (Instant salt by Aquarium Systems), in deionized water [27] and the exposure solution was renewed every 14 days. By using this method, the seawater composition and salinity remained the same all over the testing period. The pH of the attacked solution was not controlled as the seawater has a pH of 8.2 and it is known to be a tampon solution where the pH is maintained [27,38]. Two salinities were investigated in this study, namely 35 and 70 g/Kg. The exposure solution of 35 g/Kg salinity could not be renewed between day 42 and day 110 due to laboratory closure during the Covid19 pandemic.

Reference samples, immersed in tap water, were also used to distinguish the hydration effects from the seawater attack. Exposure solutions compositions are summarized in Table 2. All the samples and the solutions were stored in a room at a controlled temperature of 20 °C.

Table 2: Exposure [27] *and reference solutions composition.*

	Seawater – Salinity 35 g/L Values in mg/L			**Tap Water Values in mg/L**
Elements	**Natural Seawater**	**Recomposed seawater Provider data**	**Recomposed seawater Measured**	
Chloride	19,497	19,251	18,894	59.8
Sodium	11,049	10,757	10,861	32.0
Sulfate	2,750	2,659	2,259	18.3
Magnesium	1,318	1,317	1,293	4.7
Calcium	422	398	369	42.0
Potassium	408	402	376	3.6
Brome	67	2.30	-	-
Strontium	8.10	8.60	17	-
Borates	25.30	32.40	26.50	-
Fluor	1.30	<0.05	0.00	-

2.3. Methods of investigation

2.3.1. Macroscopic and mechanical evaluation

During exposure, samples degradation was evaluated by weekly measuring the length and weight evolution in exposure solution and at saturated-surface dried (SSD) conditions (Fig. 2). Volume and radius evolutions were calculated. Length variations were measured between the two gage studs or the central perforation of the two plates for the plain and hollow samples, respectively.

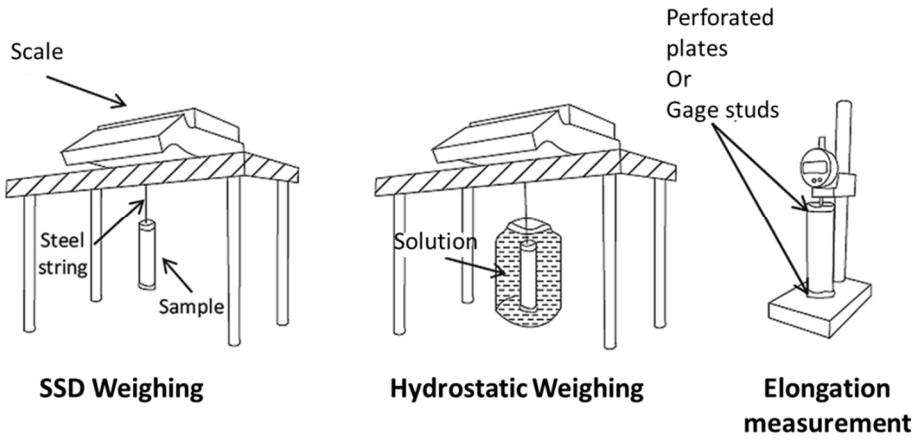

Fig. 2: Apparatus used for macroscopic evolution monitoring

To determine the compressive strength, the samples were cut at the two ends and ground to obtain a flat loading surface and a total height of 140 mm (to comply with the ASTM recommendation height=2xDiameter). Three samples were tested at the age of 1, 2, 7, 28, and 145 days and the average compressive strength was determined. During the compressive test, the load was applied at a rate of 0.5 MPa/s until failure.

The static elastic modulus was determined on two samples at the age of 1, 2, 7, 28, and 145 days using an extensometer and LVDT sensors by loading and unloading the specimen up to a load equal to 30% of its strength.

The elastic modulus evolution was determined weekly on the plain cylinders used for length monitoring using a dynamic testing method and *Grindosonic* apparatus. By creating a slight shock on the specimen, the device allows determining two natural frequencies related to the vibration created. The elastic modulus is then determined from these frequencies and the density of the specimen using the Spinner and Teft model [39]. A relationship can therefore be determined between the static and the dynamic elastic modulus. This allows determining the evolution of static Young's modulus during the exposure period.

2.3.2. Microscopic evaluation

The analysis of microstructural evolutions was performed on cement paste because in the case of mortars or concretes the presence of aggregates makes this type of analysis difficult or not significant due to the local influence of the chemical composition of aggregates. Consequently, cement paste samples were cast with a w/c ratio of 0.5.

Scanning electron microscopy (SEM) visualizations and energy dispersive spectroscopy (EDS) analysis were carried out on polished cement paste samples. The cylindrical specimens were first transversally cut then embedded in a low-modulus epoxy resin and finally polished. This cross section allowed observing the specimens from the surface exposed to seawater to the center of the sample. The pressure in the specimen chamber was 50 Pa and the accelerating voltage was 20kV. The observations were performed by backscattered electrons imaging. The elemental mappings were obtained under a magnification of 100× to 400x. Using this technique, the variations of atomic proportions could be determined from the surface to the center of the cylinder. Combining SEM and EDS helps identify the phases formed at the surface of the specimen and distinguish them from the phases formed at the center.

Thermogravimetric (TGA) analysis was performed on cement paste crushed to powders in a dry nitrogen atmosphere with a Netzsch SRA449 F3 apparatus. The samples were heated from 20 to 900 °C at a constant rate of 10°C/min. Therefore, the leaching and formation of phases due to seawater attack was identified and quantified. A comparison was made between specimens from the surface exposed to seawater and the center as well. An example of TGA/DTG analysis performed, at the age of 28 days, at the surface of resistant cement paste (PM) is presented in Fig. 3 for both reference and degraded samples. Based on the derivative thermogravimetric (DTG) curves, brucite and calcium hydroxide (CH) were characterized and quantified by the peaks at 390 - 400 °C and 460 - 510 °C, respectively. As for calcium carbonate, it can be identified at 3 peaks at 600 - 800 °C (Aragonite, Vaterite, and Calcite).

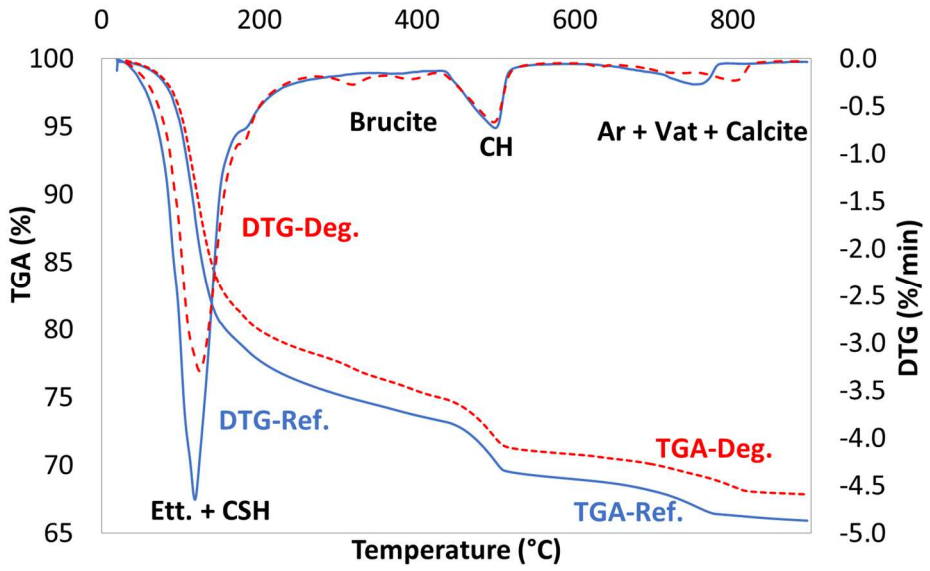

Fig. 3: TGA/DTG analysis performed, at the age of 28 days, at the surface of resistant cement paste (PM) for both reference (Ref.) and degraded (Deg.) samples

X-ray diffraction (XRD) analysis was used to identify crystalline phases qualitatively. The analyses were performed using an Aeris XRD at 30 kV. A Cu Kα source (λ1 = 1.5405980 Å and λ2 = 1.5444260 Å) with a 0.38 mm slit was used. The scan was performed between 7° and 70°. XRD analysis concerned cement paste crushed to powders and sieved at 80 µm. Similar to TGA, XRD analysis was performed on the surface (0- 2 mm) and the center of the cement pastes samples.

3. Results and discussion

As previously mentioned, the aim of the tests was to monitor the degradation of the mortar due to seawater exposure at macroscopic and microscopic levels to correlate both types of evolutions. The results are divided into three parts as follows: macroscopic characterization, microscopic characterization, and mechanical evaluation.

3.1. Macroscopic characterization

In this section, the difference between attacked and reference samples (Deg.-Ref.) is presented to eliminate the hydration evolution effect and focus solely on the seawater attack. It is actually assumed that the exposure conditions do not significantly influence the remaining hydration (after exposure time) in most part of the sample.

3.1.1. Variation of the surface dry sample weight

The graphs in Fig. 4 and Fig. 5 illustrate the difference in weight variation at SSD conditions between the attacked (Deg.) and the reference (Ref.) samples for hollow and plain specimens $((\Delta M_{SSD}/M_{ini,SSD})deg - (\Delta M_{SSD}/M_{ini,SSD})ref)$ fully immersed in both exposure solutions.

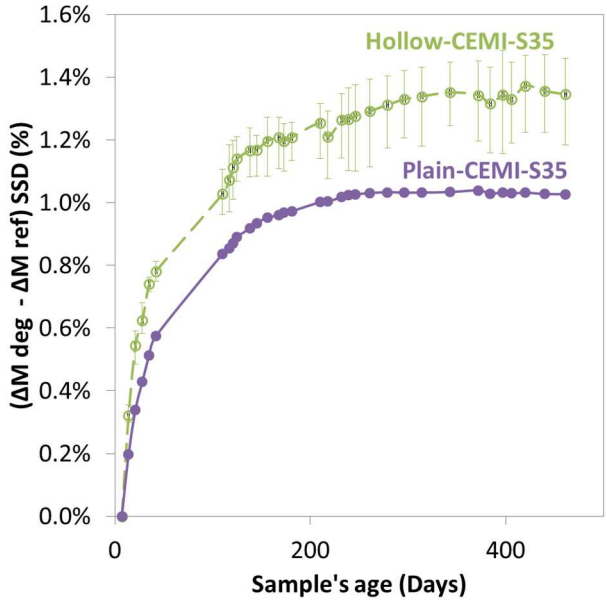

Fig. 4: Weight variations of mortar specimens at SSD conditions in seawater of salinity S=35g/L (difference between attacked and reference specimens).

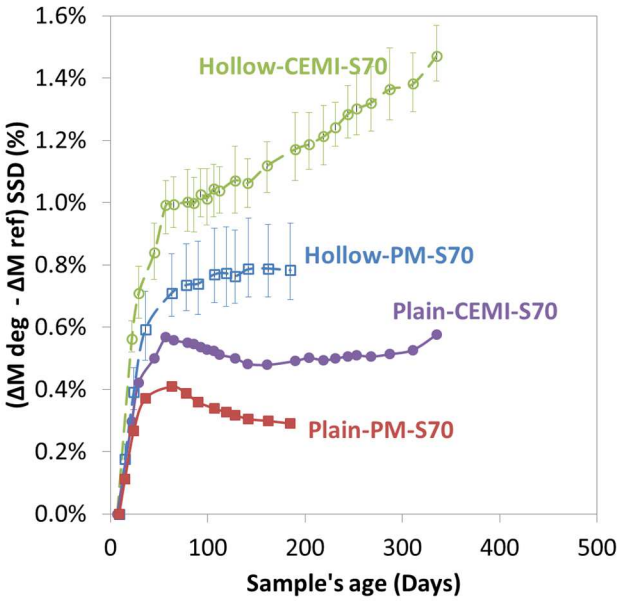

Fig. 5: Weight variations of mortar specimens at SSD conditions in seawater S=70g/L (difference between attacked and reference specimens).

The increase in weight indicates therefore a material gain due to seawater attack. Error bars are also plotted on these graphs. They were calculated as the difference between minimum and maximum and the mean of individual values measured on three specimens.

A sharp increase in the samples weight can be observed at early age for all cases then the mass starts to stabilize except for hollow samples cast with OPC (CEMI 52.5 N) and immersed in 70 g/L seawater solution as they were still recording a significant weight increase. This increase could confirm the lower stability of ordinary cement CEMI 52.5N observed at higher salinity.

In 70g/L seawater solution, the highest weight gain (1.4%) was observed on hollow samples made with non-resistant cement (CEMI). 1% weight growth was recorded for plain samples immersed in the solution having a salinity of 35 g/L. The lowest weight increase (0.5% for CEMI and 0.3% for CEM I PM) was recorded for plain samples immersed in 70 g/L.

The CEMI-S35 and CEMI-S70 results cannot be directly compared due to the period when the solutions of CEM I-S35 could not be renewed. This explains why they are not plotted on the same graph. The comparison of both graphs also shows the influence of the solution renewal on the mass evolution. Renewing the solution maintain a high gradient of ionic concentrations thus it fosters the diffusion of ionic species and leaching of cement paste. The influence of leaching on mass loss has been evidenced through the decrease of calcium content in cement paste exposed to seawater [40]. Leaching of calcium hydroxide and the decalcification of C–S–H has been reported in previous studies. If the solution is not renewed, an equilibrium can be reached between the seawater solution and the pore solution at the surface of mortar samples, which favors the precipitation of new phases. This could explain the higher mass increase observed in Fig. 4. The hollow specimens recorded the highest amount of product formation and especially in the case of mortars made with ordinary cement.

3.1.2. Volume variations and longitudinal deformation

The graphs plotted in Fig. 6 and Fig. 7 display the difference in the volume variation between the attacked and the reference samples for hollow and plain specimens ($\Delta V/V_{ini}deg - \Delta V/V_{ini}ref$) immersed in 35g/L and 70 g/L solutions. As previously mentioned, volume is calculated. It is determined by subtracting the mass in water from the mass at SSD conditions and taking into account the density of the solution.

All the specimens first recorded a rapid rise in volume and then the variation stabilized. Hollow cylinders recorded the highest volume increase and the plain samples showed a much lower volume gain. Considering the samples immersed in seawater S=70g/L (Fig. 6) the volume gain

can be classified as follows: Hollow-CEMI > Hollow-PM> Plain-CEMI > Plain-PM. This order clearly highlights the effect of cement type and samples geometry on the volume growth due to seawater attack.

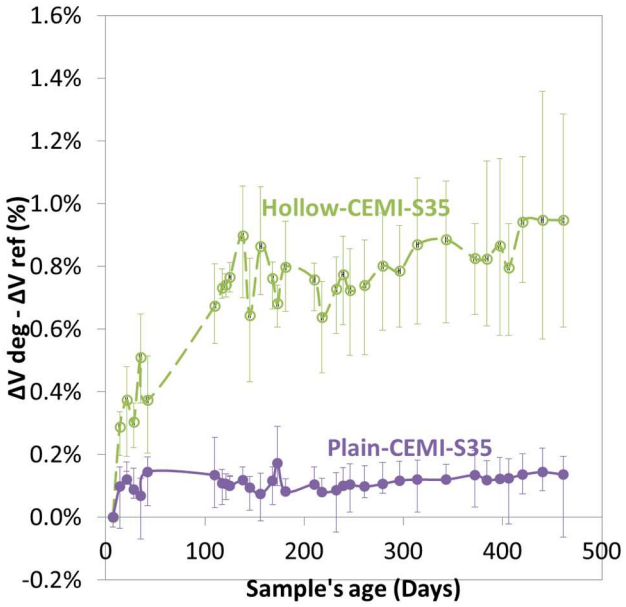

Fig. 6: Volume variations of mortar specimens in in seawater S=35g/L (difference between attacked and reference specimens).

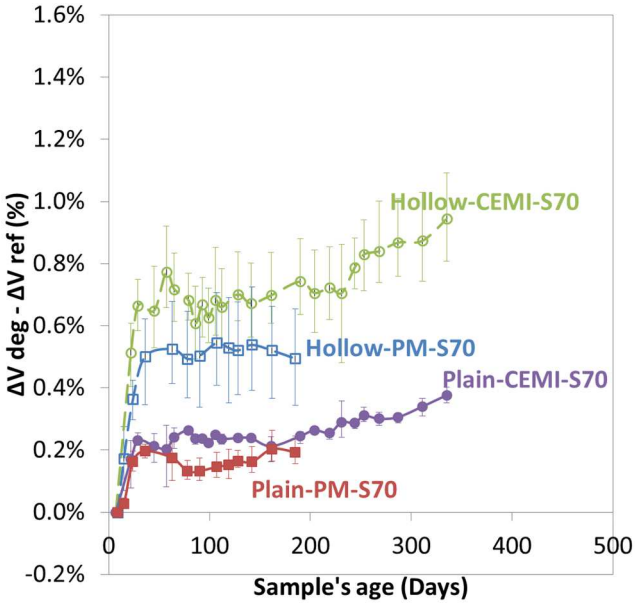

Fig. 7: Volume variations of mortar specimens in seawater S=70g/L (difference between attacked and reference specimens).

This volume gain can be explained by the precipitation of new phases and/or the stresses and expansion due to crystallization pressures induced by ettringite formation for example. At this stage, it is not possible to conclude. Further analysis and microscopic evolutions are needed to better understand the observed macroscopic evolutions.

The relationship between length and volume variation is plotted in Fig. 8 and Fig. 9. They include the longitudinal deformation expressed as the difference between the attacked and the reference samples for hollow and plain specimens ($\Delta L/L_{ini}deg - \Delta L/L_{ini}ref$) immersed in 35g/L and 70 g/L solutions. Even though specimens immersed in 70g/L solution (Fig. 9) presented little length variations for both cement types, it can still be observed that hollow samples recorded the highest length increase and the plain samples made with resistant cement (PM) recorded the lowest length gain.

An increase in length was observed ($\Delta L/L_{ini} \geq 0$) for the hollow specimens immersed in a 35 g/L solution (Fig. 8), implying an expansion of the specimens, while plain samples showed a decrease in the specimen length ($\Delta L/L_{ini} \leq 0$) thus indicating a contraction, which could be attributed to autogenous shrinkage. It is noteworthy that all measured expansions remained relatively low. They were significantly lower than the expansion reported by Santhanam et al. [13]. The Portland cement used in their experiment actually had higher C_3A content of 9% and higher C_3S content of 62% hence higher Sadran's index of 25.7, thus the data seem to support the relevance of this index. In the present study, measured expansions were also below the criteria given for the expansion induced by external sulfate attacks for instance. Lipus [41] gave a criterion of 0.07% after 9 months for assessing sulfate resistant types of cement.

The length increase did not exceed 5% of the values of volume gain. These results show that the length variation was much lower than the volume variation. Thus it can be assumed that the volume gain was due to the formation of new phases at the surface of specimens, rather than macroscopic expansion and surface leaching typically observed during external sulfate attack for example in [30]. The experimental data also show the relative stability of PM cement-based mortar, even if hollow cylinders showed higher length and volume increase. This can be considered as an acceleration as characteristic time associated with diffusion is lower for hollow specimens.

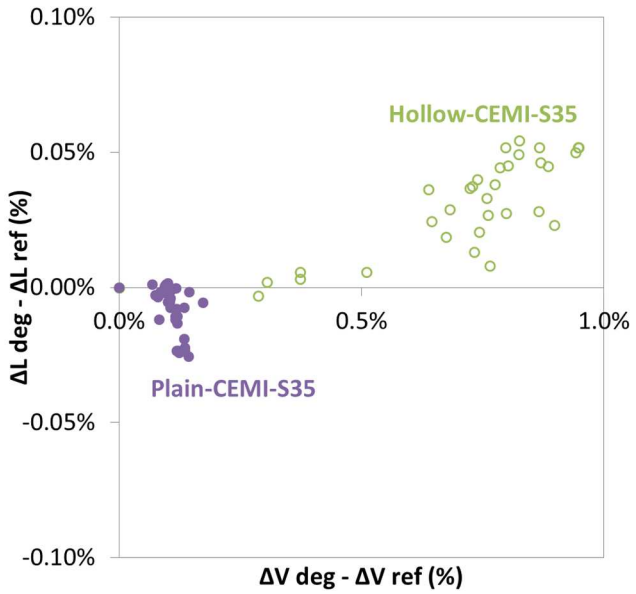

Fig. 8: Relation between length volume variation for mortar sample in S=35g/L (difference between attacked and reference specimens).

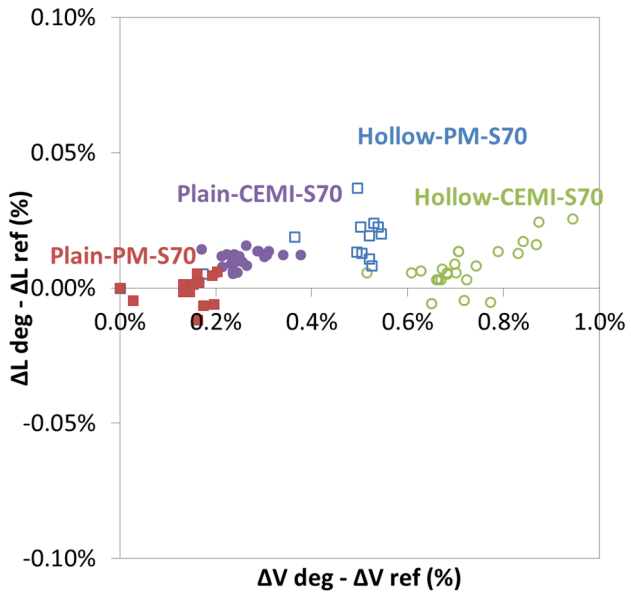

Fig. 9: Relation between length volume variation for mortar sample in S=70g/L (difference between attacked and reference specimens).

3.1.1. Products formation evolution

Fig. 10 and Fig. 11 display the differences in the equivalent thickness variation of the products deposited on the attacked and the reference samples for hollow and plain specimens ($\Delta Edeg - \Delta Eref$) immersed in 35g/L and 70 g/L solutions.

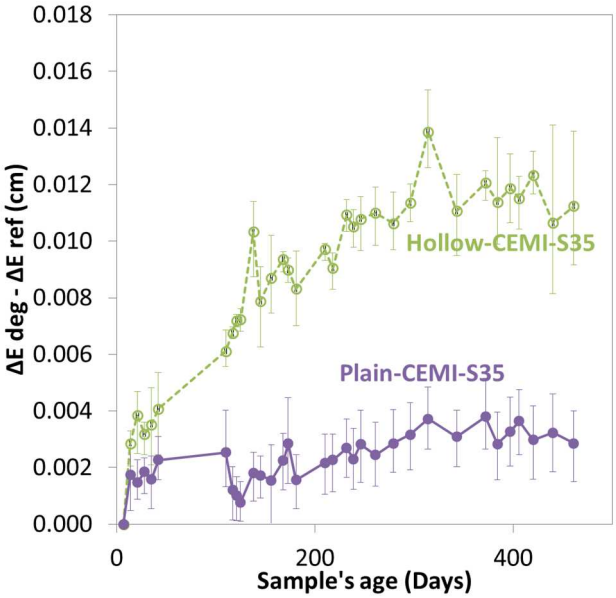

Fig. 10: Variation of the product's thickness deposited for the mortar specimens in S=35 g/L seawater (difference between attacked and reference specimens).

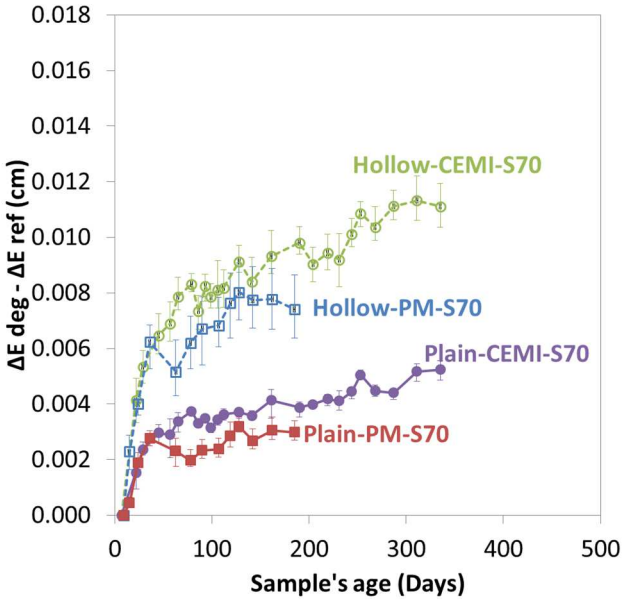

Fig. 11: Variation of the product's thickness deposited for the mortar specimens in S=70 g/L seawater (difference between attacked and reference specimens).

All samples recorded a positive thickness for the product formed at the surface exposed to seawater attack. Therefore, solid products were formed and deposited on the surface, and their thickness increased with the exposure time. For a given cement type and salinity, hollow samples recorded the highest amount of products formed. This result can be related to the weight variation at SSD conditions (Fig. 4 and Fig. 5). Hollow specimens actually showed a continuous increase in mass, thus the precipitation was more intense than leaching. This could be favored by

thicker surface deposit as indicated by Fig. 10, which possibly formed a protective layer mitigating further dissolution. Conversely, plain cylinders had lower thickness and their mass showed a slight decrease after the initial sharp increase.

By considering the same salinity (Fig. 11), mortar samples made with ordinary cement recorded a higher thickness of product formed than those cast with resistant (PM) cement (in both geometries: hollow and plain cylinders). This supports the sea-resistant character of the CEMI-PM cement.

3.2. Microscopic characterization

Fig. 12 presents SEM analysis for the polished cross sections of the exposed and reference cement paste samples made with OPC CEMI 52.5 N. Small rosette shaped crystals could be observed at the surface of the exposed samples in the early stages of attack. They can be attributed to Brucite $Mg(OH)_2$ [42,43].

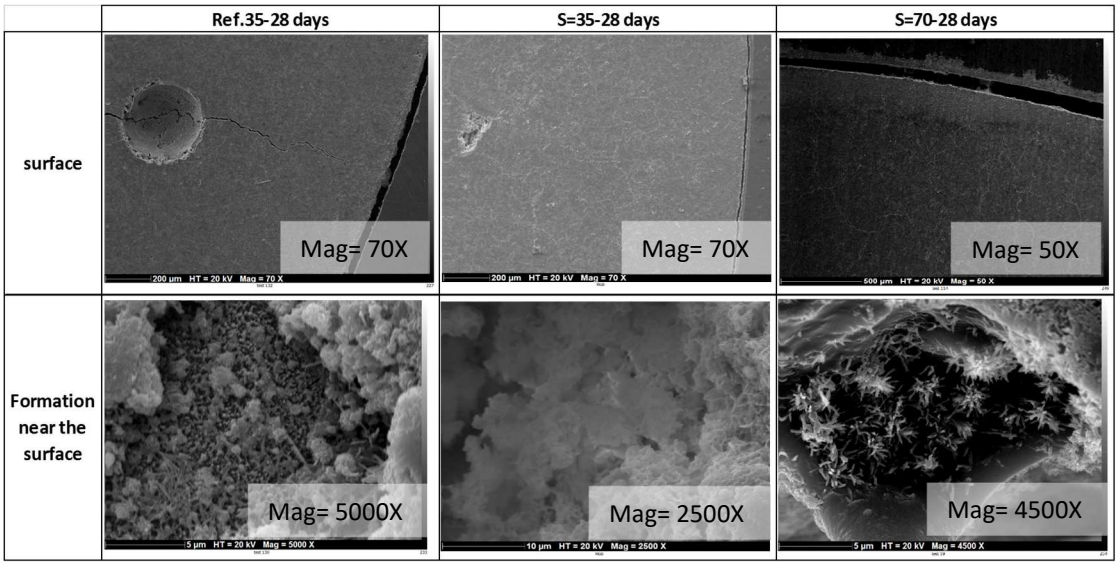

Fig. 12: SEM images of the polished specimen's surface made with CEMI 52.5 N at the age of 28 days (a. Reference sample, CEMI sample immersed in b. 35 g/L solution c. 70 g/L solution).

Fig. 13 shows SEM and Mg and Ca relative concentrations extracted from the EDS analysis. Magnesium ions are likely to form brucite from the decomposition of calcium hydroxide (Portlandite) according to equation (1).

$$Mg^{2+} + Ca(OH)_2 \rightarrow Mg\ (OH)_2 + Ca^{2+} \quad (1)$$

A high concentration of Mg can be observed as a deposited layer on the attacked specimen surface (Fig. 13). The brucite layer deposited on the exposed surface can act as an insoluble and possibly protective layer for the concrete [14]. $Mg(OH)_2$ precipitation near the surface is frequently observed in magnesium-rich environments [44] as a result of base exchange reaction (equation 1). The highest Mg concentration was identified at the surface of the sample immersed in seawater with a salinity of 70 g/L. This could be attributed to the higher salinity of 70 g/L thus higher Mg^{2+} ions concentration allowing the calcium hydroxide to further react with the Mg^{2+} ions present in the solution and this accelerated the brucite formation. The formation of the brucite layer confirms the macroscopic analysis and the interpretation of equivalent thickness variations plotted in Fig. 8 and Fig. 9. Higher magnesium concentration was also found in cement paste near the surface (Fig. 13). This could correspond to M-S-H formed from C-S-H by ion exchange of Ca by Mg [40]. Brucite can also be found intermixed with the M-S-H.

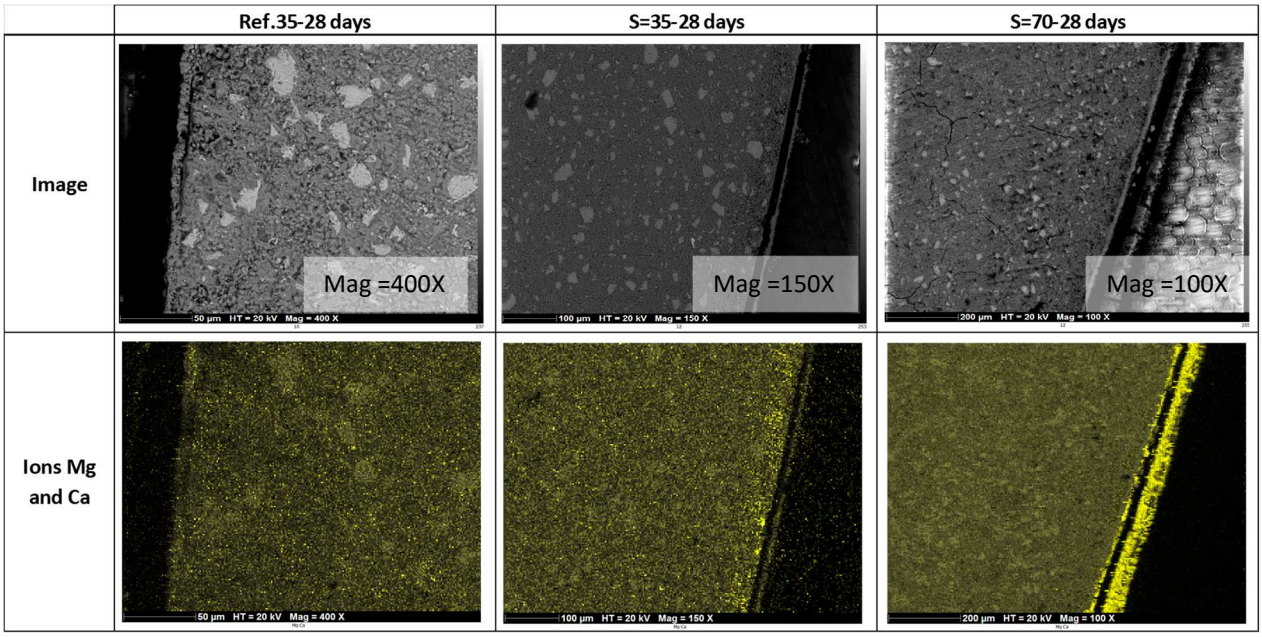

Fig. 13: SEM and EDS analysis for Mg and Ca elements of the polished specimens made with CEMI 52.5 N at the age of 28 days (a. Reference sample, Sample immersed in b. 35 g/L solution c. 70 g/L solution).

Based on the derivative thermogravimetric (DTG) curves, brucite and calcium hydroxide were characterized and quantified by the peaks at 390 - 400 °C and 460 - 510 °C, respectively. The amount of brucite and calcium hydroxide was calculated by multiplying the weight loss at each peak by 58.32/18.02 (molar mass of $Mg(OH)_2$ / molar mass of H_2O) and 74.09/18.02 (molar mass of $Ca(OH)_2$ / molar mass of H_2O), respectively. The brucite and calcium hydroxide

variation at the exposed surface is presented in Fig. 14. Calcium carbonate ($CaCO_3$) can be detected by three peaks from 600 to 800 °C (Aragonite, Vaterite, and Calcite). The amount of $CaCO_3$ is found by multiplying the weight loss at each peak by 100.087/44.009 (molar mass of $CaCO_3$ / molar mass of CO_2). The total amount of $CaCO_3$ formed at the exposed surface is presented in Fig. 15.

The SEM-EDS findings are in good agreement with the identification of the phases provided by the thermogravimetric analyses (TGA) performed at the exposed surface of the specimens. The calcium hydroxide content in the attacked specimens was lower than in the reference samples in both seawater solutions supporting the assumption that calcium hydroxide was leached from the sample surface during the seawater attack.

The graph in Fig. 14 also clearly indicates that brucite formation was not detected in the reference samples, but brucite was present in the attacked specimens. This provides some evidence that a stable brucite layer was formed at the surface of the attacked specimen. The rapid formation of brucite during the first 30 days can be correlated with the initial increase of equivalent thickness and initial mass and volume increase observed during the same period. Then the brucite content near the surface stabilized, while the calcium hydroxide content continued to decrease in the degraded specimens. This suggests that calcium hydroxide was continuously leaching and was involved in the formation of new phases. For instance, the formation of ettringite and Friedel's salt from AFm, and the precipitation of calcium carbonate phases imply the consumption of calcium hydroxide.

From the results plotted in Fig. 15, more $CaCO_3$ was formed in the attacked specimens. This can be explained by the reaction of calcium hydroxide with the seawater environment via equation (2).

$$Ca(OH)_2 + CO_2, H_2O \rightarrow Ca\,CO_3 + 2H_2O \qquad (2)$$

Calcium carbonate was also found in control samples (Ref). In these samples, calcium carbonate quickly formed during the first 30 days then its content gradually decreased. Control samples were stored in tap water (obtained from groundwater) regularly renewed. Previous studies on groundwaters have shown that calcium carbonate can form. The carbonate ions react with free calcium ions and precipitate as calcium carbonate on the specimen surface or in pores near the surface. The stability of calcium carbonate depends on water hardness and hydro carbonate content, among other parameters. If stable, this calcium carbonate rich layer induces pore-blocking effect and mitigates leaching [45]. In specimens exposed to seawater, the calcium

carbonate content near the surface continuously increased. Its content was higher at 70 g/L salinity, probably due to higher carbonate and calcium contents. Control and attacked samples made with PM cement both showed higher calcium carbonate content (Fig. 15) but lower equivalent thickness increase than ordinary Portland. These observations suggest that PM cement-based samples could have drawn higher benefits from the pore-blocking effect of the calcium carbonate rich layer.

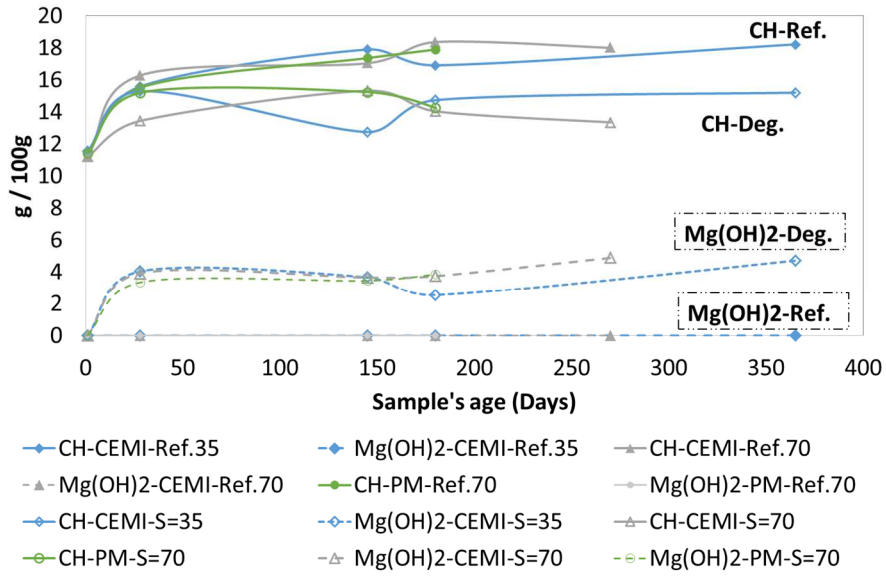

Fig. 14: Variation of brucite and calcium hydroxide present at the samples surface

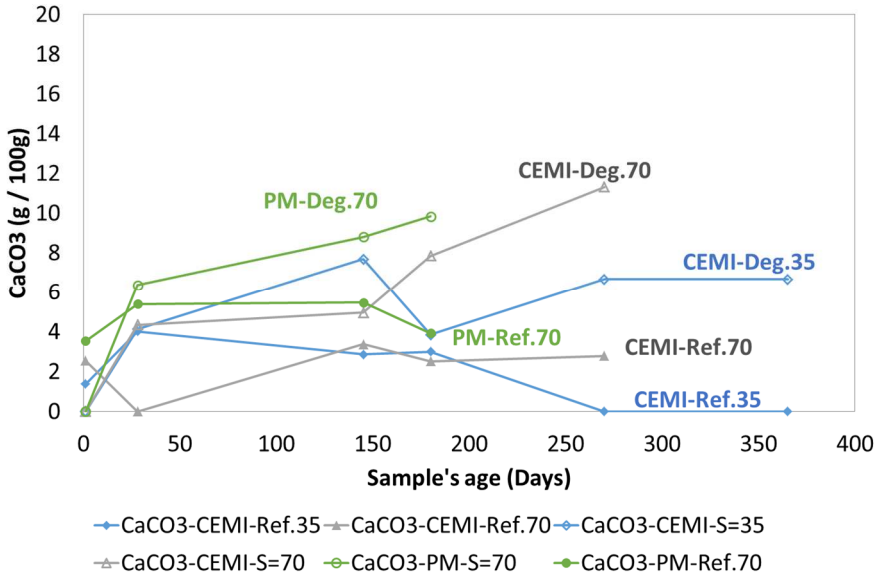

Fig. 15: Variation of calcium carbonate present at the samples surface

The XRD analysis results performed at the surface of the samples after 6-month exposure are presented in Fig. 16. They confirm the formation of brucite at the surface of samples exposed to seawater, similarly to the results obtained from TGA and SEM-EDS analysis. Brucite peak was not observed in control samples.

Friedel's salt was identified in attacked samples at the peak ($2\theta = 11.193°$) confirming the reaction of chloride ions with C_3A and $Ca(OH)_2$ (equation 3). Friedel's salt can also be formed from SO_4-AFm ($3CaO\ Al_2O_3\ CaSO_4\ 14H_2O$). In this study the mortar samples were exposed to seawater at an early age (3 days), to be representative of actual construction conditions, thus the cement was not fully hydrated at exposure time and both reactions could occur.

$$C_3A + Ca(OH)_2 + 2Cl^- + 10H_2O \rightarrow C_3A.CaCl_2.10H_2O + 2\,OH^- \qquad (3)$$

Considering the gypsum peak expected at ($2\theta = 20.731°$), gypsum could not be observed. Ettringite peak appeared in both series of samples, with no evidence that its formation was favoured in seawater. Sulfate attack generally induces expansion through crystallization pressures due to ettringite formation. Longitudinal expansion remained very low during the experiments (Fig. 8 and Fig. 9). Thus sulfate attack actually had less influence than chloride ingress in seawater. The thickness of the sulfate enriched zone has actually been reported to be much lower than the depth affected by chloride diffusion [14]. The high chloride concentration of seawater actually induces the formation of Friedel's salt from AFm, which is thus less available to form ettringite. Florea and Brouwers showed that at the chloride concentration of seawater, the total chloride binding capacity of an OPC paste can be mainly attributed to monosulfate (SO_4-AFm) and hydroxy-AFm ($C_3A{\cdot}Ca(OH)_2{\cdot}12H_2O$) [17]. The formation of ettringite in a chloride-rich system would have a reduced tendency to generate expansion, however, significant ettringite formation and expansion has been reported in seawater exposure [13], which was not the case in the present study. The expansion measurements were previously performed on thin prismatic specimens, with a thickness of 4 mm for the determination of ettringite content and 6 mm for length measurements, thus the specimens could be more affected by sulfate penetration depth than in the present study [13]. Moreover, the C_3A and C_3S contents of cement were higher, which favoured the formation of ettringite.

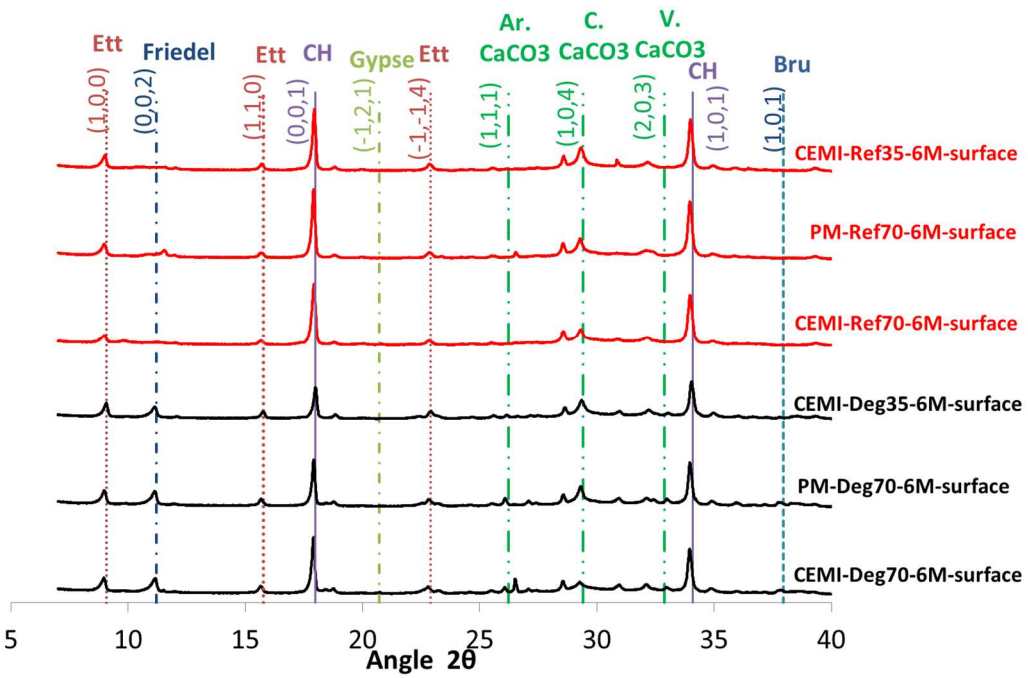

Fig. 16: XRD Patterns and (h,k,l) planes (Miller indices) observed at the specimens' surface at the age of 6 months

Aragonite and vaterite were formed at the surface of exposed specimens confirming the higher amount of $CaCO_3$ observed in TGA analysis at the exposed surface presented in Fig. 15. Aragonite and vaterite have been associated with the carbonation of C-S-H [18]. The aragonite peak can be more easily distinguished at 70 g/L salinity. The seawater would actually favour the formation of aragonite among possible calcium carbonate polymorphs [40]. Calcite was observed in both control and exposed samples. The calcite peak was clearer in PM cement than in ordinary cement. This seems consistent with TGA results (Fig. 15). The carbonation actually takes place in the outermost part of cement-based materials exposed to seawater: De Weerdt et al. observed calcium carbonate in the 0-1mm section of concrete specimens exposed to seawater for 16 years [19].

The diffraction patterns of samples after 6-month exposure are presented in Fig. 17. Friedel's salt was observed in the center of exposed samples confirming the diffusion of chloride ions inside the sample. Vaterite and aragonite were not observed at the center of exposed samples confirming that calcium carbonate precipitates at the exposed surface. Similarly, brucite was not observed in the center of the specimens confirming that the brucite layer was formed at the surface. These findings are in agreement with the results of previous studies [14].

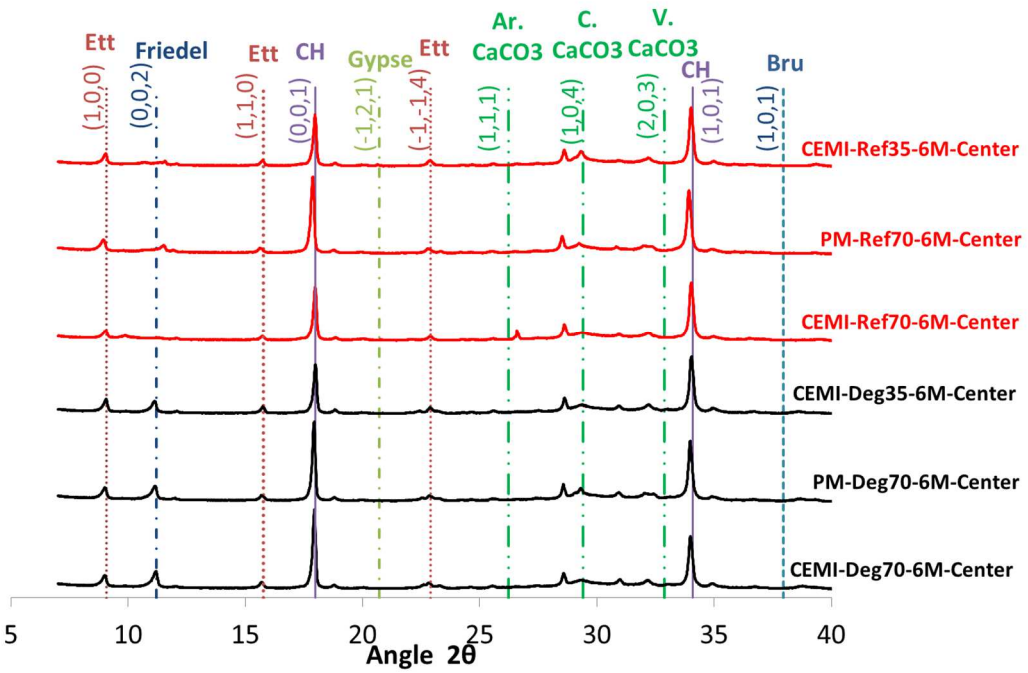

Fig. 17: XRD Patterns and (h,k,l) planes (Miller indices) observed at the specimens center at the age of 6 months

The graphs of Fig. 18 show the variations of chloride and sulfur concentrations from the exposed surface to the center of the paste samples. The penetration of chloride ions in OPC paste sample was relatively fast (Fig. 18.a). After 28 days the Cl content vs. depth curves looked like diffusion profile then Cl content significantly increased and after 6 months the profile was almost homogeneous with a slight decrease close to the surface, probably due to leaching and lower pH in this zone. These results could explain why Friedel's salt could be clearly distinguished in XRD analyses in the center of specimens (Fig. 17). The evolution of sulfate content was significantly different. Il slightly increased in the first millimetres, but it remained close to the initial sulfate content of cement paste, and no significant increase could be observed after 1 year. These results corroborate XRD data indicating no major ettringite or gypsum formation even near the surface (Fig. 16). They could also explain why no significant expansion occurred during the experiment (Fig. 8 and Fig. 9), as sulphate-rich phases and especially ettringite are associated with the macroscopic expansion in cement-based materials exposed to sulfate attack and seawater attack.

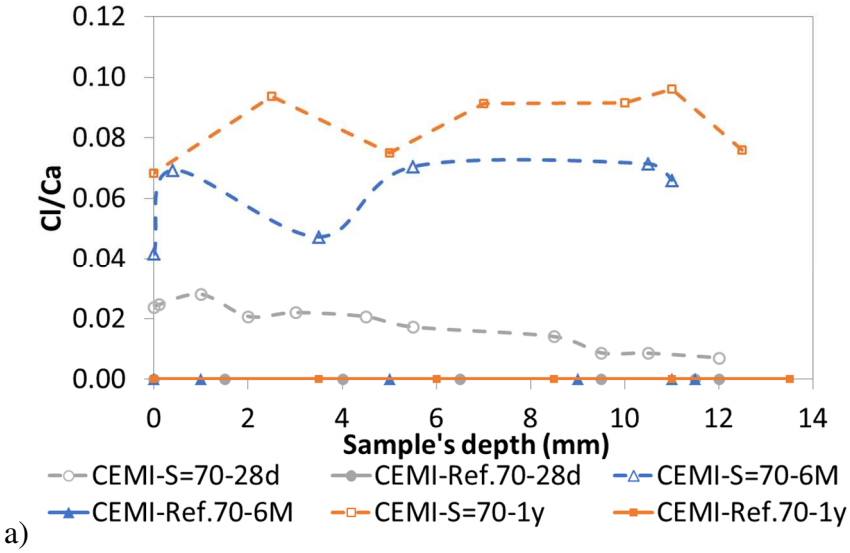

a)

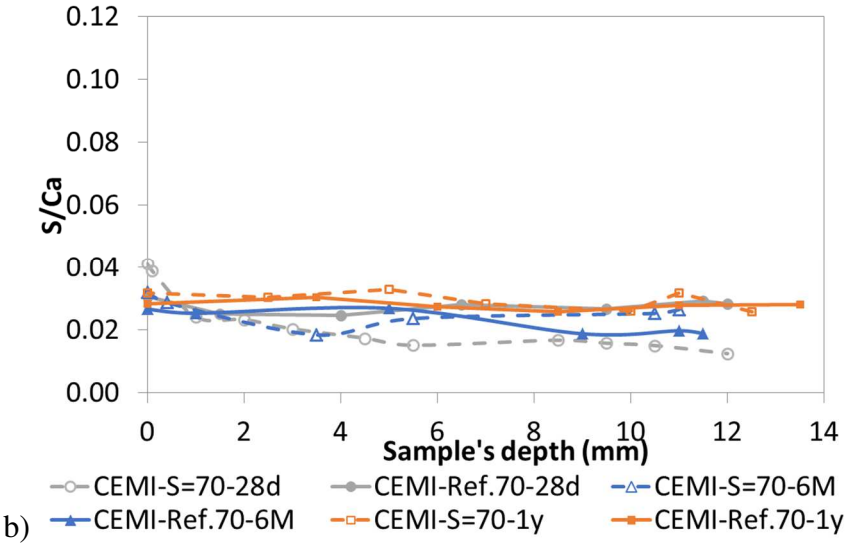

b)

Fig. 18: Chloride (Cl) and Sulphur (S) concentration profiles deduced from SEM-EDS analyses (at the age of 28 days (28d), 6 months (6M) and one year (1y).

3.3. Mechanical Evaluation

The graph in Fig. 19 shows the average compressive strength (on 3 tested specimens) at each age of testing (1, 2, 7, 28, and 145 days) and the static Young's modulus evolution during exposure.

The compressive strength of the attacked specimens remained equal or slightly lower than the resistance of control specimens even if significant evolutions could be observed at both microscopic and macroscopic levels. The chemical evolutions were mainly observed during the first weeks then the monitored parameters were mostly stable indicating the blocking effect of brucite and calcium carbonate-rich layer which mitigated subsequent macroscopic degradation of the specimens. Leaching appeared to develop continuously, as indicated by Fig. 15, which could

affect the strength in the long-term. The reference specimens made with OPC CEMI52.5N recorded the highest Young's modulus and the specimens immersed in seawater recorded the lower modulus. PM cement-based mortars exposed to tap water and seawater had the same Young's modulus.

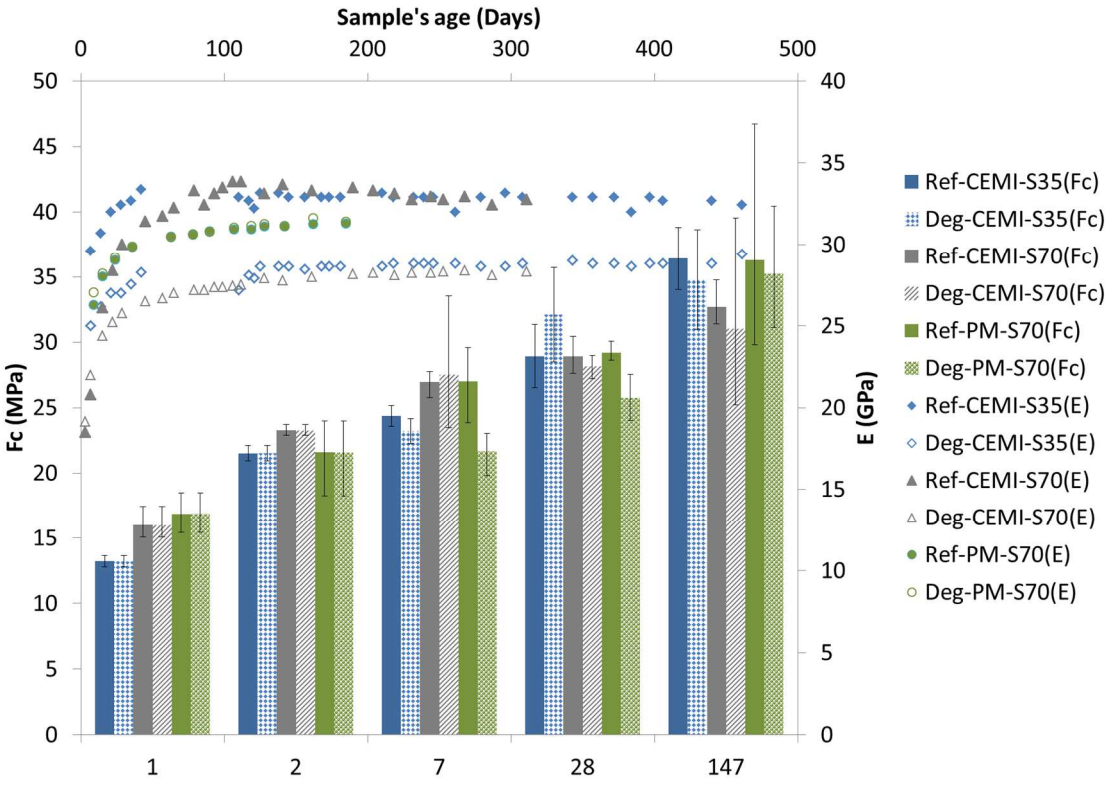

Fig. 19: : Mechanical evolutions.

The compressive strength of the mortars exposed to seawater showed a continuous increase, which was not observed in several previous studies on Portland cement-based materials. Santhanam et al. actually observed a significant relative decrease in the strength of mortar samples within 32 weeks [13]. As previously mentioned, their C_3A content and Sadran's index were higher and the specimens size was lower, which could have accelerated their deterioration. Li et al. exposed specimens to artificial seawater from 28 days to 180 days [46]. The strength of OPC-based samples increased up to 90 days then decreased. The used OPC had a relatively high C_3A content of 10%. Ghassemi and Toufigh [47] also reported an increase in compressive strength up to 6 months then a decrease; the chemical composition of the used OPC was not given. Yigiter et al. [48] also observed a decrease in strength, their OPC had high C_3A content and Sadran's index of 8.9% and 25.5, respectively. This would confirm the influence of C_3A content and Sadran's index on the mechanical properties of Portland cement-based materials

exposed to seawater. Similar to our findings, Rashad and Oudashowed reported continuous strength increase in seawater for blended cement pastes made with PC (CEMI of grade 42.5 N) and modified with solely MK, solely Q-P (quartz powder) and their combination during their immersion time [21]. Another resemblance is that the strength of the specimens in seawater remained lower than the strength of cement pastes immersed in tap water. This study highlighted the importance of the incorporation of 20% Q-P in the blends because it resulted in the lowest strength deterioration [21]. The seawater used in this study was delivered from the Mediterranean sea in the Alexandria region, Egypt, and not reformulated in the laboratory.

The present study differs from previous ones due to the cement type, W/C ratio and exposure age. Hosam El-Din H. Seleem et al. [29] studied the strength evolutions for concrete specimens, cast with CEMI 42,5 and W/C= 0.32 (with and without pozzolans additions), initially water-cured for 28 days, and then immersed in synthetic seawater till the age of testing (at 3 months, 6 months, and 12 months). For plain cement specimens, a strength increase was observed at the age of 6 months followed by a decrease at the age of 12 months. In addition, Islam M S et al. [28] have studied the sea water effect on concrete durability by immerging the concrete samples in seawater solutions after 28 days of water curing.

In this study the mortars were exposed to seawater at 3 days, thus coupling between cement hydration and seawater attack could exist. Concrete mixtures including seawater have been studied. Wang et al. [49] reported the enhanced hydration of ordinary Portland cement with seawater mixing. Cement pastes prepared with seawater reached significantly higher strength. They showed a significant formation of Friedel's salt, and calcium carbonate. The C_3A content and Sadran's index of used cement were respectively 7.2% and 25.2. Guo et al. [20] observed that the strength of seawater sea-sand concretes decreased with the increase of total ion concentration in mixing water. The hydration was accelerated at early-age but a more porous microstructure was formed. However compressive strength and elastic modulus kept increasing with time and they had the same global mechanical behavior. He and Zhou [50] combined internal sea salt attack from mixing materials and immersion in solution with 8 times the salinity of seawater. In the submerged zone, the elastic modulus increased then decreased, and the degradation was attributed to expansion associated with ettringite and gypsum formation for external seawater attack. Friedel's salt and ettringite were actually shown to be stable phases at high chloride concentrations [51,52]. Furthermore, this study has showed the accelerated hydration with seawater mixing, the stability of calcium hydroxide, and lower C-S-H content.

4. Conclusions

This study aimed to perform a comprehensive characterization of cement-based materials exposed to seawater solution by combining all the ions constituting the natural seawater. The effect of the seawater salinity, cement type and samples geometry on the mortar degradation was identified. The following conclusions can be drawn:

- At the early stages of exposure, a rapid rise in weight, volume, and radius variation was observed in all cases, then the evolutions stabilized.
- Only the mass and volume of hollow cylinders cast with ordinary Portland cement CEMI 52.5N and immersed in seawater solution of 70 g/L salinity did not stabilize.
- The highest evolutions (weight and volume gain, and the amount of products formed) were recorded for hollow cylinders specimens exposed to seawater attack. Their area of exposure was higher than the plain cylinders, allowing the ions to diffuse in both directions. Therefore, it can be concluded that hollow specimens are beneficial to shorten the response time of durability testing.
- All the specimens showed an increase in the equivalent thickness of the surface layer, confirming the formation of new products on the exposed surface. Phases formed at the surface of the exposed specimens were calcium carbonate that precipitates as aragonite and vaterite, and a brucite stable layer.
- Salinity increase did not result in significant expansions, even in the case of the hollow cylinders. Sulfate attack in seawater environments was not predominant, and the pore-blocking effect of brucite and calcium carbonate formation near the surface could have slowed down the ionic diffusion into the cement matrix.
- The lowest macroscopic evolutions has been recorded in the case of plain cylinders cast with seawater resistant cement (PM) according to Sadran's index. The mechanical properties of the attacked specimens remained equal or slightly lower than the properties of the reference specimens even if significant microstructural changes and chloride ingress have been observed at the microscopic level. From the comparison between types of cement in the present study, and previous studies, Sadran's index appeared interesting to anticipate the sensitivity of mechanical properties to seawater exposure.

Acknowledgements

The “Ecole Centrale de Nantes” and the “Lebanese University” supported financially Marinelle El-Khoury’s PhD thesis. The authors would like to thank “Vicat group” for providing the cements used in the experimental study.

References

[1] Davies RJ, Almond S, Ward RS, Jackson RB, Adams C, Worrall F, et al. Oil and gas wells and their integrity: Implications for shale and unconventional resource exploitation. Mar Pet Geol 2014;56:239–54. https://doi.org/10.1016/j.marpetgeo.2014.03.001.

[2] Zhang X, Zuo G, Memon SA, Xing F, Sun H. Effects of initial defects within mortar cover on corrosion of steel and cracking of cover using X-ray computed tomography. Constr Build Mater 2019;223:265–77. https://doi.org/10.1016/j.conbuildmat.2019.06.172.

[3] Sun H, Jiang C, Cao K, Yu D, Liu W, Zhang X, et al. Monitoring of steel corrosion and cracking in cement paste exposed to combined sulfate–chloride attack with X-ray microtomography. Constr Build Mater 2021;302:124345. https://doi.org/10.1016/j.conbuildmat.2021.124345.

[4] Cheng S, Shui Z, Gao X, Yu R, Sun T, Guo C, et al. Degradation mechanisms of Portland cement mortar under seawater attack and drying-wetting cycles. Constr Build Mater 2020;230:116934. https://doi.org/10.1016/j.conbuildmat.2019.116934.

[5] Cheng S, Shui Z, Gao X, Lu J, Sun T, Yu R. Degradation progress of Portland cement mortar under the coupled effects of multiple corrosive ions and drying-wetting cycles. Cem Concr Compos 2020;111:103629. https://doi.org/10.1016/j.cemconcomp.2020.103629.

[6] Massaad G, Roziere E, Loukili A, Izoret L. Advanced testing and performance specifications for the cementitious materials under external sulfate attacks. Constr Build Mater 2016;127:918–31. https://doi.org/10.1016/j.conbuildmat.2016.09.133.

[7] Cefis N, Comi C. Damage modelling in concrete subject to sulfate attack. Frat Ed Integrita Strutt 2014;8:222–9. https://doi.org/10.3221/IGF-ESIS.29.19.

[8] Ragoug R, Metalssi OO, Barberon F, Torrenti JM, Roussel N, Divet L, et al. Durability of cement pastes exposed to external sulfate attack and leaching: Physical and chemical aspects. Cem Concr Res 2019;116:134–45.

https://doi.org/10.1016/j.cemconres.2018.11.006.

[9] Harrison WH. Effect of chloride in mix ingredients on sulphate resistance of concrete. Mag Concr Res 1990;42:113–26. https://doi.org/10.1680/macr.1990.42.152.113.

[10] Zhang M, Chen J, Lv Y, Wang D, Ye J. Study on the expansion of concrete under attack of sulfate and sulfate – chloride ions. Constr Build Mater 2013;39:26–32. https://doi.org/10.1016/j.conbuildmat.2012.05.003.

[11] Al-Amoudi OSB, Maslehuddin M, Abdul-al Y. AB. Role of chloride ions on expansion and strength reduction in plain and blended cements in sulfate environments. Constr Build Mater 1995;9:25–33.

[12] Weerdt K De, Lothenbach B, Geiker MR. Comparing chloride ingress from seawater and NaCl solution in Portland cement mortar. Cem Concr Res 2019;115:80–9. https://doi.org/10.1016/j.cemconres.2018.09.014.

[13] Santhanam M, Cohen M, Olek J. Differentiating seawater and groundwater sulfate attack in Portland cement mortars. Cem Concr Res 2006;36:2132–7. https://doi.org/10.1016/j.cemconres.2006.09.011.

[14] De Weerdt K, Justnes H, Geiker MR. Changes in the phase assemblage of concrete exposed to sea water. Cem Concr Compos 2014;47:53–63. https://doi.org/10.1016/j.cemconcomp.2013.09.015.

[15] Touil B, Ghomari F, Khelidj A, Bonnet S, Amiri O. Durability assessment of the oldest concrete structure in the Mediterranean coastline: The Ghazaouet harbour. Mar Struct 2022;81:1–19. https://doi.org/10.1016/j.marstruc.2021.103121.

[16] Guillon E. Durabilité des matériaux cimentaires: modélisation de l'influence des équilibres physico-chimiques sur la microstructure et les propriétés mécaniques résiduelles. École Normale Supérieure de Cachan, 2004.

[17] Florea MVA, Brouwers HJH. Chloride binding related to hydration products: Part I: Ordinary Portland Cement. Cem Concr Res 2012;42:282–90. https://doi.org/10.1016/j.cemconres.2011.09.016.

[18] Slegers PA, Rouxhet PG. Carbonation of the hydration products of tricalcium silicate. Cem Concr Res 1976;6:381–8. https://doi.org/10.1016/0008-8846(76)90101-0.

[19] De Weerdt K, Orsáková D, Müller ACA, Larsen CK, Pedersen B, Geiker MR. Towards the understanding of chloride profiles in marine exposed concrete, impact of leaching and

moisture content. Constr Build Mater 2016;120:418–31. https://doi.org/10.1016/j.conbuildmat.2016.05.069.

[20] Guo M, Hu B, Xing F, Zhou X, Sun M, Sui L, et al. Characterization of the mechanical properties of eco-friendly concrete made with untreated sea sand and seawater based on statistical analysis. Constr Build Mater 2020;234:117339. https://doi.org/10.1016/j.conbuildmat.2019.117339.

[21] Rashad AM, Ouda AS. Effect of tidal zone and seawater attack on high-volume fly ash pastes enhanced with metakaolin and quartz powder in the marine environment. Microporous Mesoporous Mater 2021;324:111261. https://doi.org/10.1016/j.micromeso.2021.111261.

[22] Millero FJ, Feistel R, Wright DG, McDougall TJ. The composition of Standard Seawater and the definition of the Reference-Composition Salinity Scale. Deep Res Part I Oceanogr Res Pap 2008;55:50–72. https://doi.org/10.1016/j.dsr.2007.10.001.

[23] Millero FJ. History of the equation of state of seawater. Oceanography 2010;23:18–33. https://doi.org/10.5670/oceanog.2010.21.

[24] Lewis EL. The practical salinity scale of 1978 and its antecedents. IEEE J Ocean Eng 1980;5:350–7. https://doi.org/10.1080/15210608209379432.

[25] Feistel R. Thermodynamic properties of seawater, ice and humid air: TEOS-10, before and beyond. Ocean Sci 2018;14:471–502. https://doi.org/10.5194/os-14-471-2018.

[26] UNESCO. The International System of Units (SI) in Oceanography. Unesco Tech Pap Mar Sci 1985;31:124.

[27] Roziere E. Etude de la durabilité des matériaux cimentaires en milieu marin – Study on the durability of cement-based materials in marine environment, Internal report of FUI MAREVA project, In French. Nantes: 2012.

[28] Islam MS, Mondal BC, Islam MM. Effect of sea salts on structural concrete in a tidal environment. Aust J Struct Eng 2010;10:237–52. https://doi.org/10.1080/13287982.2010.11465048.

[29] Seleem HEDH, Rashad AM, El-Sabbagh BA. Durability and strength evaluation of high-performance concrete in marine structures. Constr Build Mater 2010;24:878–84. https://doi.org/10.1016/j.conbuildmat.2010.01.013.

[30] Boudache S, Rozière E, Loukili A, Izoret L. Towards common specifications for low- and

high-expansion cement-based materials exposed to external sulphate attacks. Constr Build Mater 2021;294:123586. https://doi.org/10.1016/j.conbuildmat.2021.123586.

[31] NF EN 206-1. Béton - Spécification, performance, production et confirmité - Complément national à la norme NF EN 206. AFNOR; 2014.

[32] Justnes H. Thaumasite formed by sulfate attack on mortar with limestone filler. Cem Concr Compos 2003;25:955–9. https://doi.org/10.1016/S0958-9465(03)00120-3.

[33] Lee ST, Hooton RD, Jung HS, Park DH, Choi CS. Effect of limestone filler on the deterioration of mortars and pastes exposed to sulfate solutions at ambient temperature. Cem Concr Res 2008;38:68–76. https://doi.org/10.1016/j.cemconres.2007.08.003.

[34] Rilem. Rapport sur les résultats d'une enquête internationale de la RILEM sur les essais et recherches relatifs au comportement des ciments dans les ouvrages à la mer. Matériaux Constr 1970;3.

[35] ASTM C150. 04a, Standard specification for Portland cement. 2002.

[36] EN196-1:2016. Methods of testing cement. Determination of strength. 2016.

[37] Feely RA, Doney SC, Cooley SR. Ocean acidification - Present conditions in a high-CO2 World. Oceanography 2009;22:21–40. https://doi.org/10.1017/cbo9781139198776.020.

[38] Lide DR. CRC Handbook of Chemistry and Physics, 84th edition. CRC Press; 2004. https://doi.org/10.1136/oem.53.7.504.

[39] Spinner E, Tefft WE. A method for determining mechanical resonance frequencies and for calculating elastic moduli from these frequencies. Proc. ASTM, 1961.

[40] De Weerdt K, Justnes H. The effect of sea water on the phase assemblage of hydrated cement paste. Cem Concr Compos 2015;55:215–22. https://doi.org/10.1016/j.cemconcomp.2014.09.006.

[41] Lipus K. VDZ approach for testing SR cements, RILEM TC-251 SRT. Extern. Sulfate Attack Work., Madrid: 2018.

[42] Grattan-Bellew PE. Microstructural investigation of deteriorated Portland cement concretes. Constr Build Mater 1996;10:3–16. https://doi.org/10.1016/0950-0618(95)00066-6.

[43] Ragab AM, Elgammal MA, Hodhod OAG, Ahmed TES. Evaluation of field concrete deterioration under real conditions of seawater attack. Constr Build Mater 2016;119:130–44. https://doi.org/10.1016/j.conbuildmat.2016.05.014.

[44] Brown PW, Doerr A. Chemical changes in concrete due to the ingress of aggressive species. Cem Concr Res 2000;30:411–8. https://doi.org/10.1016/S0008-8846(99)00266-5.

[45] Hartwich P, Vollpracht A. Influence of leachate composition on the leaching behaviour of concrete. Cem Concr Res 2017;100:423–34. https://doi.org/10.1016/j.cemconres.2017.07.002.

[46] Li G, Zhang A, Song Z, Shi C, Wang Y, Zhang J. Study on the resistance to seawater corrosion of the cementitious systems containing ordinary Portland cement or/and calcium aluminate cement. Constr Build Mater 2017;157:852–9. https://doi.org/10.1016/j.conbuildmat.2017.09.175.

[47] Ghassemi P, Toufigh V. Durability of epoxy polymer and ordinary cement concrete in aggressive environments. Constr Build Mater 2020;234:117887. https://doi.org/10.1016/j.conbuildmat.2019.117887.

[48] Yiğiter H, Yazici H, Aydin S. Effects of cement type, water/cement ratio and cement content on sea water resistance of concrete. Build Environ 2007;42:1770–6. https://doi.org/10.1016/j.buildenv.2006.01.008.

[49] Wang J, Liu E, Li L. Multiscale investigations on hydration mechanisms in seawater OPC paste. Constr Build Mater 2018;191:891–903. https://doi.org/10.1016/j.conbuildmat.2018.10.010.

[50] He X, Zhou J. Mechanical characteristics of sea-sand concrete in simulated marine environment. Constr Build Mater 2021;274. https://doi.org/10.1016/j.conbuildmat.2020.122098.

[51] Balonis M, Lothenbach B, Le Saout G, Glasser FP. Impact of chloride on the mineralogy of hydrated Portland cement systems. Cem Concr Res 2010;40:1009–22. https://doi.org/10.1016/j.cemconres.2010.03.002.

[52] Li P, Li W, Yu T, Qu F, Tam VWY. Investigation on early-age hydration, mechanical properties and microstructure of seawater sea sand cement mortar. Constr Build Mater 2020;249:118776. https://doi.org/10.1016/j.conbuildmat.2020.118776.